Antiferromagnetic Transitions of Osmium-containing Rare Earth Double Perovskites Ba_2LnOsO_6 (Ln = Rare Earths)

Yukio Hinatsu*, Yoshihiro Doi and Makoto Wakeshima

Division of Chemistry, Hokkaido University, Sapporo 060-0810, Japan

Corresponding author, tel/fax:+81-11-706-2702

E-mail address: hinatsu@sci.hokudai.ac.jp

Keywords: Magnetic properties; Perovskite; Osmium; Rare earth; Specific heat, Mössbauer spectrum

Abstract

The perovskite-type compounds containing both rare earth and osmium Ba_2LnOsO_6 (Ln = Pr, Nd, Sm-Lu) have been prepared. Powder X-ray diffraction measurements and Rietveld analysis show that Ln^{3+} and Os^{5+} ions are structurally ordered at the M site of the perovskite $BaMO_3$. Magnetic susceptibility and specific heat measurements show that an antiferromagnetic ordering of Os^{5+} ions has been observed for Ba_2LnOsO_6 (Ln = Pr, Nd, Sm, Eu, Gd, Lu) at 65-71 K. Magnetic ordering of Ln^{3+} moments occurs when the temperature is furthermore decreased.

1. Introduction

One of the most challenging problems in the modern chemistry of rare earth compounds is to find a compound in which strong magnetic superexchange interactions between 4f electrons exist, which give rise to a long-range magnetic ordering at relatively high temperatures, and to elucidate their mechanism. We have been focusing our attention on the crystal structures of the perovskite-type compounds containing rare earth ions. The rare earth ion is relatively large and tends to adopt a high coordination number. Therefore, the rare earth ion usually sits at the A site of the perovskite-type oxides ABO_3. Not the A site ions but the B site ions normally determine the physical properties of the perovskites [1]. The perovskites have the flexibility of chemical composition and the possibility of combination of many kinds of ions. By selecting large alkaline earth elements such as Sr and Ba at the A site atoms, one finds that the rare earths occupy the 6-coordinate B sites. Double perovskite-type oxides have the formula $A_2B'B''O_6$, in which the primes indicate the different ions in different oxidation states, and the cations at the B-sites, B' and B", are regularly ordered, i.e., 1:1 arrangement of B' and B" ions has been observed over the six-coordintate B sites. Different kinds of B' and B" ion should show a variety of the physical properties of double perovskite oxides.

The solid-state chemistry of such mixed-metal oxides containing platinum group metals has attracted a great deal of interest. The preparation, crystal structures and magnetic properties of double perovskite oxides containing Ru ion, A_2LnRuO_6 (A = alkali-earth metals), where Ln represents a rare earth ion, have been studied [2-14]. The electronic configuration of Ru^{5+} is $[Kr]4d^3$ ([Kr]: krypton electronic core), which means that it has the largest spin (S = 3/2). Such highly oxidized cations from the second or third transition series sometimes show quite unusual magnetic behavior. Any of the double perovskites Ba_2LnRuO_6 (Ln = La ~ Lu) [2, 4, 5, 9-12] and Sr_2LnRuO_6 (Eu ~ Lu) [3, 4, 6-8, 12-14] show an antiferromagnetic transition at low temperatures, and the transition temperature is higher than that for the compounds in which the magnetic ion at the B site is Ru^{5+} ion only. Among them, the transition temperature for

Ba_2PrRuO_6 is astonishingly as high as 117 K [10], and Ba_2NdRuO_6 transforms to the antiferromagnetic state at 57 K [9].

Recently, magnetic properties of pentavalent osmium-containing oxides have aroused a great deal of interest, because the Os^{5+} ion has the largest possible spin (S = 3/2) [15-18]. The magnetic properties of Ba_2LnOsO_6 are expected to be quite different from those of other double perovskite oxides Ba_2LnMO_6 (M = Ru, Ir, Re), because in general, the effect of M^{5+} ions on the magnetic properties of Ba_2LnMO_6 should be larger than that of Ln^{3+} ions. However, the magnetic properties of Ba_2LnOsO_6 were not studied. Treiber et al. reported the preparation of the Ba_2LnOsO_6 and their lattice parameters [19]. No detailed crystal structures nor magnetic properties were reported. We reported magnetic properties of neodymium-containing osmium double perovskite Ba_2NdOsO_6.The magnetic moment of Os^{5+} orders at 65 K and then the antiferromagnetic ordering of Nd^{3+} occurs at a lower temperature ~20 K from the magnetic and specific heat measurements [20]. Magnetic properties of $NaOsO_3$ and La_2NaOsO_6 with the perovskite-type structure are also worth noting. $NaOsO_3$ has a metal-insulator transition driven by magnetism [21], and the magnetic properties of La_2NaOsO_6 are characterized by a drastically-reduced Os ordered moment due to magnetic frustration [22].

Concerning the preparation of osmium-containing oxides, Plaisier and IJdo reported that it is difficult to control the oxidation state of osmium in oxides by using oxygen donor reactants [16]. For the case of Ba_2LnOsO_6, when both OsO_2 and Os metal are available as starting materials, double perovskites Ba_2LnOsO_6 could be prepared by the following reaction:

$$2BaO_2 + 1/2Ln_2O_3 + 1/4OsO_2 + 3/4Os \rightarrow Ba_2LnOsO_6. \quad (1)$$

That is, we need not use oxygen donors such as Ag_2O and $KClO_3$ anymore, which considerably reduces the formation of volatile osmium tetroxide OsO_4.

In this study, a series of Ba_2LnOsO_6 (Ln = Pr, Sm-Lu) compounds were prepared, and their crystal structures and magnetic properties were studied through X-ray diffraction, magnetic

susceptibility, specific heat and Eu Mössbauer spectrum measurements. Here we will discussed the results on Ln = Pr, Eu, Gd and Lu compounds.

2. Experimental

2.1. Sample preparation

Polycrystalline samples of Os-bearing double perovskites Ba_2LnOsO_6 (Ln = Pr, Sm ~ Lu) were prepared by the standard solid-state reaction. Rare earth sesqui-oxides (Ln_2O_3, 99.99%, Shin-etsu Chemical), osmium dioxide (OsO_2, 99.99%, Premion from Alfa Aesar), Os metal (99.9%, Alfa Aesar), barium peroxide (BaO_2, 99.9%, Soekawa Chemicals) were used as starting materials. These starting materials were well mixed in an agate mortar. The mixtures were pressed into pellets and enwrapped with platium foils, and they were sealed in evacuated silica tubes. They were fired at 1170 K for 5 h.

2.2. X-ray diffraction analysis

Powder X-ray diffraction profiles were measured using a Rigaku Multi-Flex diffractometer with Cu-Kα radiation equipped with a curved graphite monochromator. The data were collected by step-scanning in the angle range of $10° \leq 2\theta \leq 120°$ at a 2θ step-size of 0.02°. The X-ray diffraction data were analyzed by the Rietveld technique, using the program RIETAN-FP [23] and the crystal structure was drawn by VESTA program [24].

2.3. Magnetic susceptibility measurements

The temperature-dependence of the magnetic susceptibility was measured in an applied field of 0.1 T over the temperature range of $1.8 \text{ K} \leq T \leq 400 \text{ K}$, using a SQUID magnetometer (Quantum Design, MPMS5S). The susceptibility measurements were performed under both zero-field-cooled (ZFC) and field-cooled (FC) conditions. The former was measured upon heating the sample to 400 K under the applied magnetic field of 0.1 T after zero-field cooling to 1.8 K. The latter was measured upon cooling the sample from 400 to 1.8 K in the applied field of 0.1 T.

2.4. Specific heat measurements

Specific heat measurements were performed using a relaxation technique by a commercial heat capacity measuring system (Quantum Design, PPMS) in the temperature range of 1.8-400 K. The sintered sample in the form of a pellet was mounted on a thin alumina plate with Apiezon for better thermal contact.

2.5. ^{151}Eu Mössbauer spectroscopy measurements

The ^{151}Eu Mössbauer spectra were measured with a Mössbauer spectrometer VT-6000 (Laboratory Equipment Co.) in the constant acceleration mode using a radiation source $^{151}SmF_3$ (1.85 GBq). The spectrometer was calibrated with a spectrum of α-Fe at room temperature. The γ-rays were detected with a NaI scintillation counter. Europium trifluoride (EuF_3) was used as a reference standard for the chemical isomer shift. The sample was wrapped in an aluminum foil so as to have its average surface density of 10 mg (Eu) cm^{-2}.

3. Results and Discussion

3.1. Crystal structure

The results of powder X-ray diffraction measurements show that Ba_2LnOsO_6 (Ln = Pr, Nd, Sm-Lu) compounds were formed as a single phase with perovskite-type structure. Figure 1 shows the X-ray diffraction profile for Ba_2SmOsO_6. The X-ray diffraction data collected on Ba_2LnOsO_6 could be indexed in space group $Fm\bar{3}m$ with a unit cell of size $(2a_p)^3$ (a_p: the size of a simple cubic perovskite unit cell). The diffraction line at 2θ ~ 18.2° corresponding to the 1 1 1 reflection shows that the space group is not $Pm\bar{3}m$, but $Fm\bar{3}m$. This space group allows two crystallographically distinct octahedral sites in the double perovskite structure, thus permitting 1 : 1 ordered arrangement between Sm^{3+} and Os^{5+} ions. The atomic positional parameters for Ba_2SmOsO_6 are tabulated in Table 1. Figure 2 shows the crystal structure of Ba_2SmOsO_6. For other Ba_2LnOsO_6 (Ln = Pr, Nd, Sm-Lu) compounds, the unit cell parameters and the reliability factors are listed in supplementary Table S.1.

Figure 3 shows the variation of lattice parameter for Ba_2LnOsO_6 with the ionic radius of Ln^{3+}. As the ionic radius of Ln^{3+} increases, the lattice parameter increases. The variation is nearly linear, so it is thought that the oxidation state of the rare earth is trivalent and that of osmium is pentavalent for all the compounds Ba_2LnOsO_6 (Ln = Pr, Nd, Sm-Lu). In the case that some of the rare earth ion is in the tetravalent state, the deviation from the linear relationship between the lattice parameters and the ionic radius of Ln^{3+} has been observed for Sr_2LnIrO_6 [25] and Ba_2LnIrO_6 [26].

3.2. Magnetic properties

The results of the magnetic susceptibility measurements for Ba_2LnOsO_6 (Ln = Pr, Nd, Sm-Lu) in the temperature range between 1.8 and 400 K are listed in Table 2. The Curie-Weiss law is valid for the magnetic susceptibilities of Ba_2LnOsO_6 in higher temperature ranges, except for Ba_2SmOsO_6 and Ba_2EuOsO_6. The effective magnetic moments (μ_{eff}) and Weiss constants (θ) of these compounds are listed in Table 2. The negative Weiss constant indicates that the predominant magnetic interactions in Ba_2LnOsO_6 compounds are antiferromagnetic.

Compounds with Ln = Pr, Nd, Sm, Eu, Gd and Lu show an antiferromagnetic transition at relatively high temperatures, 65-71 K, which is due to the magnetic ordering of Os^{5+} moments, as described later. Temperature dependences of the magnetic susuceptibility (reciprocal susceptibility) for Ln = Sm, Ho, Tb, Yb compounds are listed in supplementary Figs. S1 ~ S4. Ba_2HoOsO_6 shows an antiferromagnetic behaviour at 24 K. The magnetic transition temperatures for Ba_2TbOsO_6 and Ba_2YbOsO_6 are 2.6 and 2.4 K, respectively, which indicates that the magnetic transition is due to the Tb (Yb) ions, i.e., the contribution of the Os ions to the magnetic transition is neglible. Compounds with Ln = Dy, Er, and Tm are paramagnetic down to 1.8 K.

In this paper, we will mainly discuss the magnetic properties of Ln = Lu, Eu, Pr, and Gd compounds in the followings.

3.2.1. Ba_2LuOsO_6

Figure 4 shows the magnetic susceptibility vs temperature curve of Ba_2LuOsO_6 in the temperature range between 1.8 and 300 K. An antiferromagnetic behavior has been observed at 66 K. The ZFC and FC susceptibilities begin to diverse when the temperature is decreased through 66 K, i.e., Ba_2LuOsO_6 is not an ideal antiferromagnet. Small magnetic hysteresis has been observed at 5 K, and the remnant magnetization completely disappears when the temperature is increased above 66 K. That is, the antiferromagnetic interactions at low temperatures have a weak ferromagnetic component.

The inset of Fig. 4 shows the temperature dependence of the reciprocal ZFC magnetic susceptibility for Ba_2LuOsO_6. The Curie-Weiss law is valid for the magnetic susceptibility of Ba_2LuOsO_6 in the temperature range between 90 and 400 K. The effective magnetic moment (μ_{eff}) and the Weiss constant (θ) are determined to be 1.31 μ_B and -123.9K, respectively. Since the spin-orbit coupling cannot be ignored for the $5d^3$ ions, the expected moment of Os^{5+} should be lower than the spin-only value of 3.87 μ_B. Comparable lower effective magnetic moment of Os^{5+} has been observed in some Os-containing compounds [20, 27-33].

Figure 5 (a) depicts the temperature dependence of the specific heat divided by temperature (C_p/T) for Ba_2LuOsO_6 in the temperature range between 1.8 and 300 K. A specific heat anomaly has been found at the same temperature at which the magnetic susceptibility shows the antiferromagnetic transition.

In this Ba_2LuOsO_6 compound, only the Os^{5+} ions are magnetic. The magnetic entropy change (S_{mag}) associated with the magnetic ordering of Os^{5+} moments is calculated from the specific heat data. To evaluate the magnetic contribution to the specific heat (C_{mag}), we have to subtract the contribution of lattice specific heat (C_{lat}) from the total specific heat ($C_{mag} = C_p - C_{lat}$). The lattice specific heat was estimated by using the specific heat data for diamagnetic Ba_2LuTaO_6. From the temperature dependence of the magnetic specific heat, the magnetic entropy change (S_{mag}) for Ba_2LuOsO_6 is calculated by integrating the magnetic specific heat

divided by temperature (C_{mag}/T), *i.e.*, $S_{mag} = \int (C_{mag}/T)dT$. The temperature dependence of S_{mag} is shown in Fig. 5 (b). The obtained S_{mag} of Ba_2LuOsO_6 at 100 K is 3.8 J/(mol K). In an octahedral crystal field environment, the ground state of the Os^{5+} ion degenerates to four-fold. It is expected that the magnetic entropy change of Os^{5+} is $R\ln(2S + 1) = R\ln4 = 11.52$ J/(mol K), where R and S are the molar gas constant and the spin quantum number, respectively. The magnetic entropy change S_{mag} obtained experimentally is lower than that calculated. This result indicates that the beginning of the magnetic ordering of Os^{5+} moments occurs at a higher temperature.

3.2.2. Ba_2EuOsO_6

Figure 6 depicts the magnetic susceptibility vs. temperature curve for Ba_2EuOsO_6. A clear antiferromagnetic behavior has been observed at 67 K. The ground state of Eu^{3+} ion is nonmagnetic ($^7F_0$), and the excited states ^7F_J ($J = 1, 2,$ --) are above 500 K. Therefore, in the low temperature region the contribution of the Eu^{3+} ion to the magnetic properties of Ba_2EuOsO_6 is negligible, indicating that the above-mentioned magnetic properties are ascribed to the Os^{5+} ion.

Figure 7 (a) shows the temperature dependence of the specific heat (C_p) for Ba_2EuOsO_6. A clear λ-type specific heat anomaly has been observed at 67 K, which corresponds to the antiferromagnetic ordering of the Os^{5+} moments by the magnetic susceptibility measurements. The magnetic specific heat (C_{mag}) of Ba_2EuOsO_6 was estimated by subtracting the contribution of the lattice specific heat (C_{lat}) from the total specific heat (C_p). As the lattice specific heat of Ba_2EuOsO_6, we used the specific heat data of Ba_2EuTaO_6 i.e., $C_{mag} = C_{lat}(Ba_2EuOsO_6) - C_{lat}(Ba_2EuTaO_6)$. The magnetic entropy change (S_{mag}) associated with the magnetic ordering of Ba_2EuOsO_6 is calculated by integrating the magnetic specific heat divided by temperature (C_{mag}/T), *i.e.*, $S_{mag} = \int (C_{mag}/T)dT$. The temperature dependence of the C_{mag}/T and S_{mag} for Ba_2EuOsO_6 is shown in Fig. 7 (b). The obtained S_{mag} of Ba_2EuOsO_6 at 200 K is 8.5 J /(mol K).

Although this value is a little smaller than the expected S_{mag} value, 11.52 J/(mol K), we can confirm that the magnetic behavior below 67 K is due to the magnetic ordering of Os^{5+} moments.

As shown in Fig. 6, the temperature dependence of the magnetic susceptibility of Ba_2EuOsO_6 does not follow the Curie-Weiss law. The ground state of Eu^{3+} is nonmagnetic ($^7F_0$), and the excited states ^7F_J (J = 1, 2, --) are close enough to give energy differences comparable to k_BT at room temperature. Thus, the molar magnetic susceptibility for Eu^{3+} can be expressed by the following equation [34]:

$$\chi_{Eu^{3+}} = \frac{N_A {\mu_B}^2 / 3k_B}{\gamma T} \frac{24 + (13.5\gamma - 1.5)e^{-\gamma} + (67.5\gamma - 2.5)e^{-3\gamma} + (189\gamma - 3.5)e^{-6\gamma} \cdots}{1 + 3e^{-\gamma} + 5e^{-3\gamma} + 7e^{-6\gamma} + \cdots} \quad (2)$$

where the parameter $\gamma = \lambda/k_BT$ is the ratio of the multiplet width (the spin-orbit coupling constant, λ) and the thermal energy (k_BT), and γ is 1/21 for the Eu^{3+} ion. We consider that in the paramagnetic region, the magnetic behavior of the Eu^{3+} ion and Os^{5+} ion are independent of each other and that the susceptibility of Ba_2EuOsO_6 will be given by the sum of the susceptibilities of each paramagnetic ion. If we assume that the susceptibility of Os^{5+} follows the Curie-Weiss law, the total magnetic susceptibility of Ba_2EuOsO_6 will be given by

$$\chi(Ba_2EuOsO_6) = \frac{C}{T - \theta} + \chi_{Eu^{3+}} + \chi_{TIP} \quad (3)$$

where C is the Curie constant of Os^{5+} and χ_{TIP} is the temperature independent susceptibility of Ba_2EuOsO_6. In order to explain the behavior of magnetic susceptibility and to estimate the effective magnetic moment (μ_{eff}) and Weiss constant (θ) of Os^{5+}, we attempted to fit this equation to experimental magnetic susceptibilities. By fitting, we have obtained λ = 374(1) cm^{-1}, μ_{eff} = 1.10 (3) μ_B, and θ = -71.4 (38) K. This λ value is comparable to the values reported in other double perovskites, for example, 364 cm^{-1} for Sr_2EuIrO_6 [35] and 339 cm^{-1} for Ba_2EuNbO_6 [36].

Figure 8 (a) shows the ^{151}Eu Mössbauer spectra of Ba_2EuOsO_6 measured at 80 K. A single absorption peaks appeared at δ = 1.16 mm/sec, indicating that the Eu ion is in the trivalent state.

Because of the low symmetry of the Eu sites in Ba_2EuOsO_6, the electric field gradient tensor should exist and the nonzero quadrupole interaction is expected at the Eu sites. The quadrupole Hamiltonian is given by

$$H_Q = \frac{e^2qQ}{4I(2I-1)}\left(3I_z^{\,2} - I(I+1) + \eta(I_x^{\,2} + I_y^{\,2})\right) \qquad (4)$$

where I is the nuclear spin, Q is the quadrupole moment, $eq = V_{zz}$, and the asymmetric parameter $\eta = (V_{xx} - V_{yy}) / V_{zz}$ (V_{ii} is the electric field gradient tensor) [37]. Actually, the spectra exhibited a slightly asymmetric line ($\eta \neq 0$). It is impossible to fit such a spectrum with a single Lorentzian line because of the distortion due to the quadrupole interaction. The 12 possible transitions (eight allowed transitions and four forbidden transitions) (see Fig. 9) due to a quadrupole interaction were taken into account; the observed data were fitted with the sum of these Lorentzian lines (see Fig. 8 (a)). In order to derive these Lorentzian equations, the results by Shenoy and Dunlap were used [38] and the ratio of the excited and ground state quadrupole moments ($R_Q = Q_e/Q_g$) was taken as 1.312 [39]. The fitting parameters, the isomer shift (δ), the quadrupole coupling constant ($eV_{zz}Q_g$) and the asymmetry parameter (η) were determined for Ba_2EuOsO_6, and they are listed in Table 3. Comparable values of parameters are reported for Ba_2EuNbO_6 [36].

When the temperature was decreased through 50 K, the splitting due to magnetic hyperfine interactions was appeared. Figure 8 (b) shows the ^{151}Eu Mössbauer spectrum of Ba_2EuOsO_6 at 20 K. Although the ground state of Eu^{3+} is $^7F_0$, there are low-lying magnetic excited states, the $^7F_1$ state at 500 K and the $^7F_2$ state at 1500 K. In the presence of a magnetic exchange interaction with Os^{5+}, these excited states should be mixed into the ground state which produces a nonzero magnetic hyperfine field at the Eu nucleus. The magnetic hyperfine pattern is produced by transitions from the $I_g = 5/2$ ground state to the $I_e = 7/2$ excited state, and has 18 components which should overlap considerably. The results of the ^{151}Eu Mössbauer measurements at 20 K (Fig. 8 (b)) also show that we observe no full splitting at this temperature. So, it is difficult to simulate the ^{151}Eu Mössbauer spectra of Ba_2EuOsO_6 and to determine the magnetic hyperfine

field at the Eu nucleaus. However, with using the same Mössbauer parameters determined at 80 K, we tried to fit the experimental spectra measured at 20 K and obtained the magnetic hyperfine field of 19.6 T. Comparable magnetic hyperfine field has been reported for $EuSbSe_3$ [40] and Ba_2EuRuO_6 [41]. The fitting results are shown in Fig. 8 (b).

3.2.3. Ba_2PrOsO_6

Figure 10 shows the temperature dependence of magnetic susceptibilities for Ba_2PrOsO_6, indicating the occurrence of magnetic ordering at 90 K. The inset shows the temperature dependence of the reciprocal magnetic susceptibility for Ba_2PrOsO_6. The Curie-Weiss law is valid for the magnetic susceptibilities in the higher temperature range. In this compound, not only the Os^{5+} ion but also the Pr^{3+} ion is magnetic. If we assume that the magnetic moment of the Os^{5+} ion is 1.31 μ_B, the effective magnetic moments of Ba_2LnOsO_6 (μ_{calc}) should be calculated from the equation $\mu_{calc} = \sqrt{\mu_{Os^{5+}}{}^2 + \mu_{Ln^{3+}}{}^2}$. They are also listed in Table 2 and agree with the moments experimentally obtained for Ba_2LnOsO_6 (μ_{eff}).

Figure 11 (a) depicts the temperature dependence of the specific heat (C_p) for Ba_2PrOsO_6 in the temperature range between 1.8 and 200 K. A λ-type specific heat anomaly has been observed at 71 K. This temperature is a little bit lower than the Néel temperature estimated from the magnetic susceptibility measurements, and is still the highest among the Néel temperatures observed for Ba_2LnOsO_6. The same results have been reported for ruthenium-containing Ba_2LnRuO_6, i.e., the Néel temperature for Ba_2PrRuO_6 is the highest (117 K) among the Néel temperatures of Ba_2LnRuO_6 [10].

Next, we will calculate the magnetic entropy change (S_{mag}) due to the magnetic ordering of Os^{5+} and Pr^{3+} moments. The magnetic specific heat (C_{mag}) of Ba_2PrOsO_6 was estimated by subtracting the contribution of the lattice specific heat from the total specific heat in the same way as is the case for Ba_2LuOsO_6 and Ba_2EuOsO_6. The temperature dependence of the C_{mag} and

S_{mag} for Ba_2PrOsO_6 is shown in Fig. 11 (b). In addition to the λ-type anomaly at 71 K due to the magnetic ordering of the Os^{5+} moments, another specific heat anomaly is clearly observed around 20 K, which should be attributable to the antiferromagnetic ordering of the Pr^{3+} moments.

The magnetic entropy change associated with the sum of the two magnetic anomalies is determined to be ~13 J/mol K. As shown in Fig. 11 (b), it is difficult to divide the magnetic entropy data into two anomalies. The magnetic entropy change associated with the magnetic ordering of the Os^{5+} moments is estimated to be 3.8 J/mol K from the specific heat measurements for Ba_2LuOsO_6. When the same estimation for the magnetic entropy change due to the Os^{5+} moments holds for the case of Ba_2PrOsO_6, the rest of the magnetic entropy change due to the magnetic ordering of the Pr^{3+} moments is ~9.2 J/mol K. This value is close to $R\ln(1+2)$ (= 9.13J/mol K). The ground multiplet $^3H_4$ of the Pr^{3+} ion should be split into one singlet Γ_1, two doublet Γ_3, Γ_4 and one quartet Γ_5 by the crystal field in the site symmetry of *Oh* [42]. The ground state of Pr^{3+} ion is expected to be Γ_1 with the first excited state Γ_4. The results of the specific heat measurements indicate that both the doublet Γ_4 state and the ground Γ_1 state form the antiferromagnetic state of the Pr^{3+} moments because the magnetic ordering occurs at relatively high temperatures.

3.2.4. Ba_2GdOsO_6

The temperature dependence of the magnetic susceptibility for Ba_2GdOsO_6 in the temperature range between 1.8 and 300 K is shown in Fig. 12 (a). It seems that no magnetic interaction has been observed down to 1.8 K. When the $d(\chi T)/dT$ is plotted against temperature in Fig. 12 (b), a maximum is appeared at 67 K. This result indicates that an antiferromagnetic ordering of the Os^{5+} moments occur at this temperature. Paramagnetic behavior of the Gd^{3+} ions with large magnetic moments hinders the magnetic ordering of the Os^{5+} moments in the magnetic susceptibility vs temperature curve of Ba_2GdOsO_6. The temperature dependence of the reciprocal magnetic susceptibility is shown in the inset of Fig. 12 (a). The magnetic susceptibility

follow the Curie-Weiss law above 100 K. The effective magnetic moment for Ba_2GdOsO_6 is obtained to be 8.13 μ_B. This value is very close to the moment calculated from the equation $\mu_{calc} = \sqrt{\mu_{Os^{5+}}{}^2 + \mu_{Gd^{3+}}{}^2}$, as listed in Table 2.

4. Summary

A series of perovskite-type compounds containing both rare earth and osmium Ba_2LnOsO_6 have been prepared. The Ln^{3+} and Os^{5+} ions are structurally ordered at the M site of the perovskite $BaMO_3$. An antiferromagnetic transition has been observed at low temperatures. Measurements of the magnetic susceptibility, specific heat and ^{151}Eu Mössbauer measurements for Ln = Pr, Eu, Gd, and Lu compounds show that Os^{5+} moments antiferromagnetically order at around 70 K. With decreasing temperature, magnetic ordering of the Pr^{3+} moments occurs at around 20K.

References

[1] K. Ito, K. Tezuka and Y. Hinatsu, *J. Solid State Chem.*, **157**, 173-179 (2001).

[2] P.D. Battle, J.B. Goodenough, and R. Price, *J. Solid State Chem.*, **46**, 234-244 (1983).

[3] P.D. Battle and W.J. Macklin, *J. Solid State Chem.*, **52**, 138-145 (1984).

[4] P.D. Battle and W.J. Macklin, *J. Solid State Chem.*, **54**, 245-250 (1984).

[5] P.D. Battle and C.W. Jones, *J. Solid State Chem.*, **78**, 108-116 (1989).

[6] P.D. Battle, C.W. Jones, and F. Studer, *J. Solid State Chem.*, **90**, 302-312 (1991).

[7] Y. Doi and Y. Hinatsu, *J. Phys.: Condens. Matter*, **11**, 4813-4820 (1999).

[8] Y. Doi, Y. Hinatsu, K. Oikawa, Y. Shimojo, and Y. Morii, *J. Mater. Chem.*, **10**, 797-800 (2000).

[9] Y. Izumiyama, Y. Doi, M. Wakeshima, Y. Hinatsu, K. Oikawa, Y. Shimojo, and Y. Morii, *J. Mater. Chem.*, **10**, 2364-2367 (2000).

[10] Y. Izumiyama, Y. Doi, M. Wakeshima, Y. Hinatsu, Y. Shimojo, and Y. Morii, *J. Phys.: Condens. Matter*, **13**, 1303-1313 (2001).

[11] Y. Izumiyama, Y. Doi, M. Wakeshima, Y. Hinatsu, A. Nakamura, and Y. Ishii, *J. Solid State Chem.*, **169**, 125-130 (2002).

[12] Y. Hinatsu and Y. Doi, *Bull. Chem. Soc. Japan*, **7**1, 1093-1113 (2003).

[13] Y. Izumiyama, Y. Doi, M. Wakeshima, Y. Hinatsu, Y. Shimojo, and Y. Morii, *J. Phys.: Condens. Matter*, **16**, 7611-7624 (2004).

[14] R. Saez-Puche, E. Climent-Pascual, R. Ruiz-Bustos, M. A. Alario-Franco, and M. T. Fernandez-Diaz, *Progress in Solid State Chem.*, **35**, 211-219 (2007).

[15] R. Lam, F. Wiss, and J. E. Greedan, *J. Solid State Chem.* **167**, 182-187 (2002).

[16] J. R. Plaisier, R. J. Drost, and D. J. W. IJdo, *J. Solid State Chem.* **169**, 189-198 (2002).

[17] W. R. Gemmill, M. D. Smith, Y. A. Mozharivsky, G. J. Miller, and H-C, zur Loye, *Inorg. Chem.*, **44**, 7047-7055 (2005).

[18] Y. Hinatsu and Y. Doi, *J. Solid State Chem.*, **198**, 176-185 (2013).

[19] U. Treiber, S. Z. Kemmler-Sack, *Anorg. Allg.Chem*., **478**, 223-232 (1981).

[20] M. Wakeshima, Y. Hinatsu and K. Ohoyama, *J. Solid State Chem*., **197**, 236-241 (2013).

[21] S. Calder, V. O. Garlea, D. F. McMorrow, M. D. Lumsden, M. B. Stone, J. C. Lang, J.-W. Kim, J.A. Schlueter, Y. G. Shi, K. Yamaura, Y. S. Sun, Y. Tsujimoto and A. D. Christianson, *Phys. Rev. Letters*, **108**, 257209 (2012).

[22] A. A. Aczel, D. E. Bugaris, L. Li, J.-Q. Yan, C. de la Cruz, H.-C. zur Loye and S. E. Nagler, *Phys. Rev.*, **87**, 014435 (2013).

[23] F. Izumi and K. Momma, *Solid State Phenom.*, **130**, 15-20 (2007).

[24] K. Momma and F. Izumi, *Appl. Crystallogr*., **41**, 653-658 (2008).

[25] D. Harada, M. Wakeshima, and Y. Hinatsu, *J. Solid State Chem.*, **145**, 356-360 (1999).

[26] M. Wakeshima, D. Harada, and Y. Hinatsu, *J. Mater. Chem.*, **10**, 419-422 (2000).

[27] F. Abraham, J. Trehoux, and D. Thomas, *J. Inorg. Nucl. Chem.*, **42**, 1627-1630 (1980).

[28] K. E. Stitzer, A. ElAbed, M. D. Smith, M. J. Davis, S-J. Kim, J. Darriet, and H-C. zur Loye, *Inorg. Chem.*, **42**, 947-949 (2003).

[29] L. Chi, I. P. Swainson, and J. E. Greedan, *J. Solid State Chem.*, **177**, 3086-3091 (2004).

[30] K. E. Stitzer, M. D. Smith, H-C. zur Loye, *Solid State Sciences*, **4**, 311-316 (2002).

[31] W. R. Gemmill, M. D. Smith, R. Prozorov, and H-C. zur Loye, *Inorg. Chem.*, **44**, 2639-2646 (2005).

[32] K. Yamamura, M. Wakeshima, and Y. Hinatsu, *J. Solid State Chem.*, **179**, 605-612 (2006).

[33] Y. Hinatsu and Y. Doi, *J. Solid State Chem.*, **198**, 176-185 (2013).

[34] J. H. Van Vleck, *The Theory of Electric and Magnetic Susceptibilities*, Oxford University Press, London, 1931.

[35] M. Wakeshima, D, Harada, and Y. Hinatsu, *J. Solid State Chem.*, **147**, 618-623 (1999).

[36] K. Henmi and Y. Hinatsu, *J. Solid State Chem.*, **148**, 353-360 (1999).

[37] C.P.Slichter, *Principles of Magnetic Resonance*, Harper &Row, New York, 1963.

[38] G. K. Shenoy and B. D. Dunlap, *Nucl. Instr. Methods*, **71**, 285 (1969).

[39] J. G. Stevens, in "Handbook of Spectroscopy" (J. W. Robinson, Ed.), Vol. III, p. 464, CRC Press, Boca Raton, FL, 1981.

[40] F. M. Schappacher, R. Pöttgen, G. B. Jin, and T. E. Albrecht-Schmitt, *J. Solid State Chem.*, **180**, 3035-3038 (2007).

[41] T. C. Gibb and R. Greatrex, *J. Solid State Chem.*, **34**, 279-288 (1980).

[42] K. R. Lea, M. J. M. Leask, W. P. Wolf, *J. Phys. Chem.Solids*, **23**, 1381-1405 (1962).

[43] J. Van Kranendonk, J. H. Van Vleck, *Rev. Mod. Phys.*, **30**, 1-23 (1958).

Figure captions

Fig. 1 Powder X-ray diffraction profile for Ba_2SmOsO_6. The calculated profiles based on the $Fm\bar{3}m$ model and the observed profiles are shown on the top solid line and cross markers, respectively. The vertical marks in the middle show positions calculated for Bragg reflections. The lower trace is a plot of the difference between calculated and observed intensities. A diffraction line at $2\theta = 23.9°$ is due to the impurity of silicate formed by the reaction with the silica tube.

Fig. 2 Crystal structure of Ba_2SmOsO_6.

Fig. 3 Variation of lattice parameters for Ba_2LnOsO_6 (Ln = Pr, Nd, Sm-Lu) with Ln^{3+} radius.

Fig. 4 Temperature dependence of the magnetic susceptibility for Ba_2LuOsO_6 in the temperature range between 1.8 and 300 K. Blue circles are susceptibilities measured under ZFC conditions and red circles are those measured under FC conditions. The inset shows the temperature dependence of the reciprocal ZFC susceptibility for Ba_2LuOsO_6. The solid line is the Curie-Weiss fitting.

Fig. 5 (a) Temperature dependence of the specific heat divided by temperature (C_p/T) for Ba_2LuOsO_6 in the temperature range between 1.8 and 300 K. (b) Temperature dependence of the magnetic entropy change (S_{mag}) for Ba_2LuOsO_6 below 100 K.

Fig. 6 Temperature dependence of the magnetic susceptibility for Ba_2EuOsO_6 in the temperature range of 1.8 and 400 K. Open circles are susceptibilities measured under ZFC conditions and filled circles are those measured under FC conditions. A solid line is calculated with eqn. (3) (see text).

Fig. 7 (a) Temperature dependence of the specific heat (C_p) for Ba_2EuOsO_6 and Ba_2EuTaO_6 in the temperature range between 1.8 and 300 K. (b) Temperature dependence of the magnetic specific heat divided by temperature (C_{mag}/T) and magnetic entropy change (S_{mag}) for Ba_2EuOsO_6 below 200 K.

Fig. 8 (a) The ^{151}Eu Mössbauer spectra of Ba_2EuOsO_6 measured at 80 K. The red line is a calculated line with Lorentians. Green lines are the 12 Lorentzians (see text). (b) The ^{151}Eu Mössbauer spectra of Ba_2EuOsO_6 measured at 20 K.

Fig. 9 Twelve possible transitions by the quadruple interaction of ^{151}Eu nucleus.

Fig.10 Temperature dependence of the magnetic susceptibility for Ba_2PrOsO_6 in the temperature range of 1.8 and 400 K. Blue circles are susceptibilities measured under ZFC conditions and red circles are those measured under FC conditions. The inset shows the temperature dependence of the reciprocal ZFC susceptibility for Ba_2PrOsO_6. The solid line is the Curie-Weiss fitting.

Fig.11 (a) Temperature dependence of the specific heat (C_p) for Ba_2PrOsO_6 in the temperature range between 1.8 and 200 K. (b) Temperature dependence of the magnetic specific heat (C_{mag}) and magnetic entropy change (S_{mag}) for Ba_2PrOsO_6 below 100 K. The magnetic specific heat below 1.8 K was extrapolated by the relation $C_{mag} \propto T^3$ from the spin-wave model for the antiferromagnet [43].

Fig. 12(a) Temperature dependence of the magnetic susceptibility for Ba_2GdOsO_6 in the temperature range of 1.8 and 300 K. No divergence between ZFC and FC susceptibilities throughout the experimental temperature. The inset shows the temperature dependence of the reciprocal susceptibility for Ba_2GdOsO_6. A solid line is the Curie-Weiss fitting. (b) Temperature dependence of the first derivatives of χT against temperature in the neighborhood of T_N.

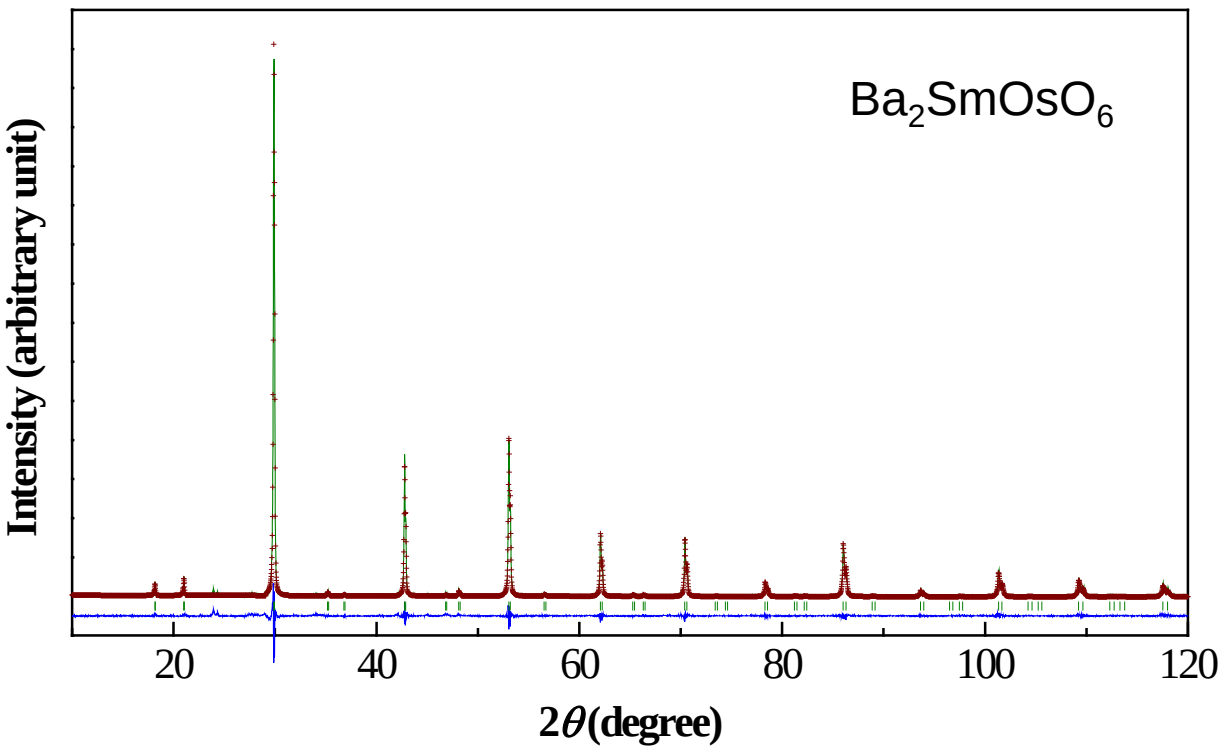
Ba2SmOsO6
Intensity (arbitrary unit)
20
40
60
80
100
120
2θ(degree)

Fig. 1

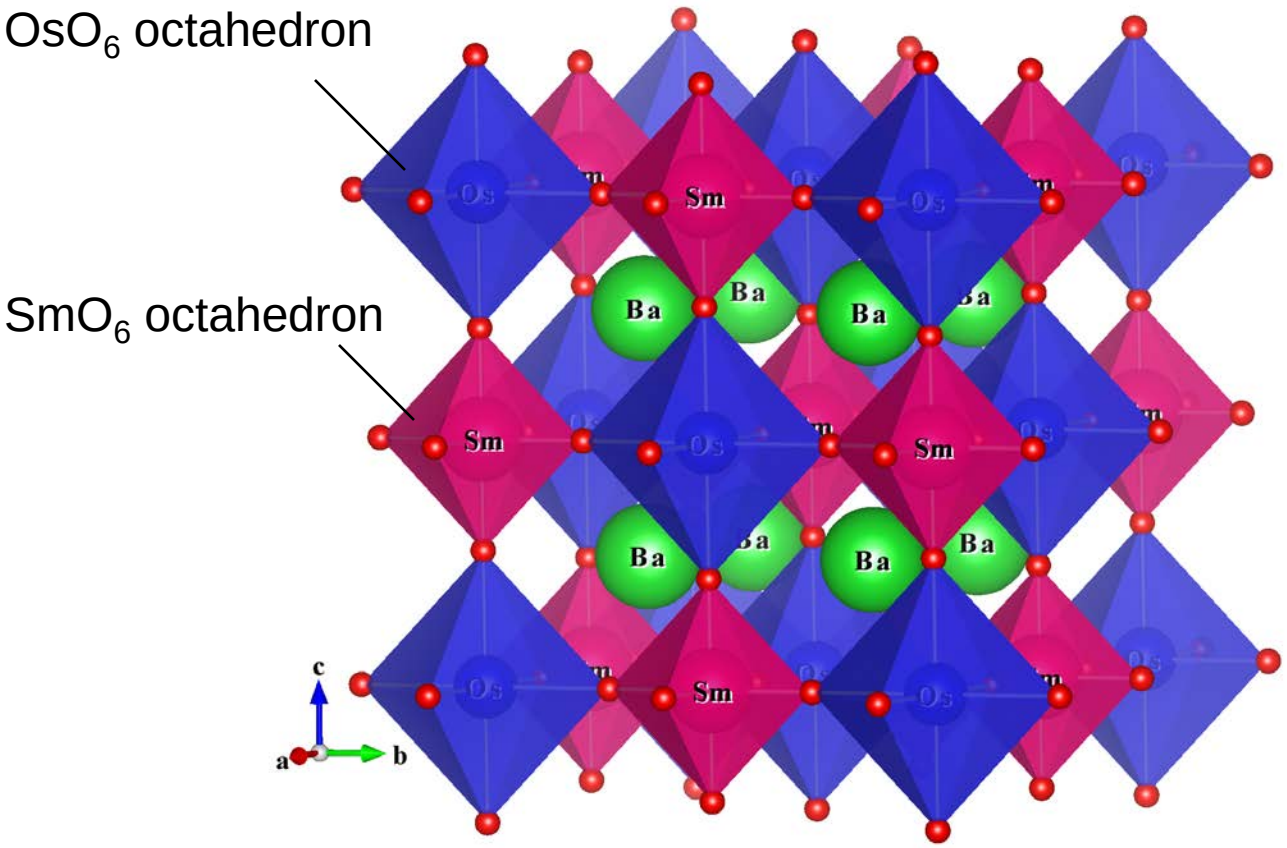

Fig. 2

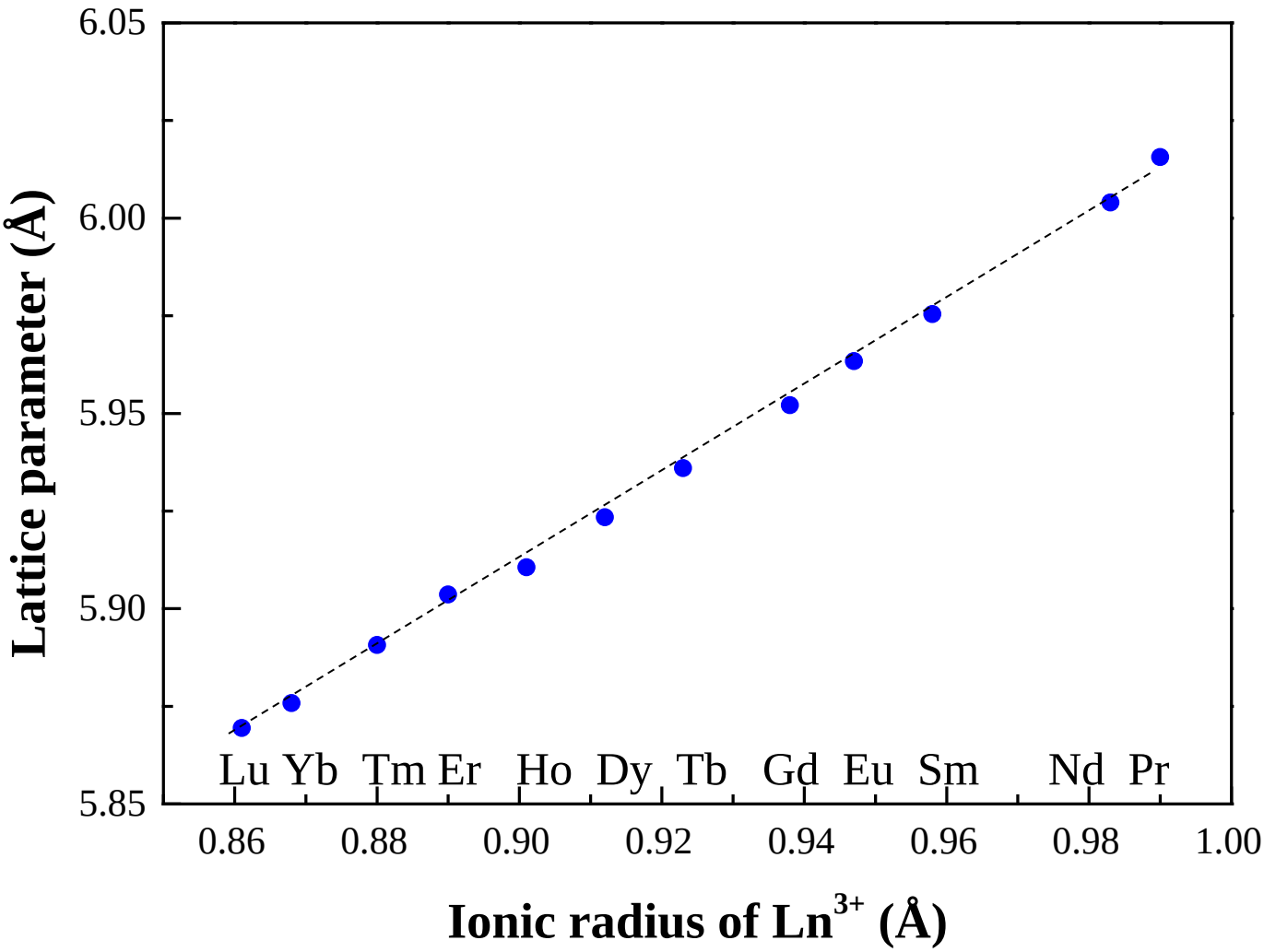
6.05
6.00
5.95
5.90
5.85
Lattice parameter (Å)
Lu Yb Tm Er Ho Dy Tb Gd Eu Sm Nd Pr
0.86
0.88
0.90
0.92
0.94
0.96
0.98
1.00
Ionic radius of Ln3+ (Å)

Fig. 3

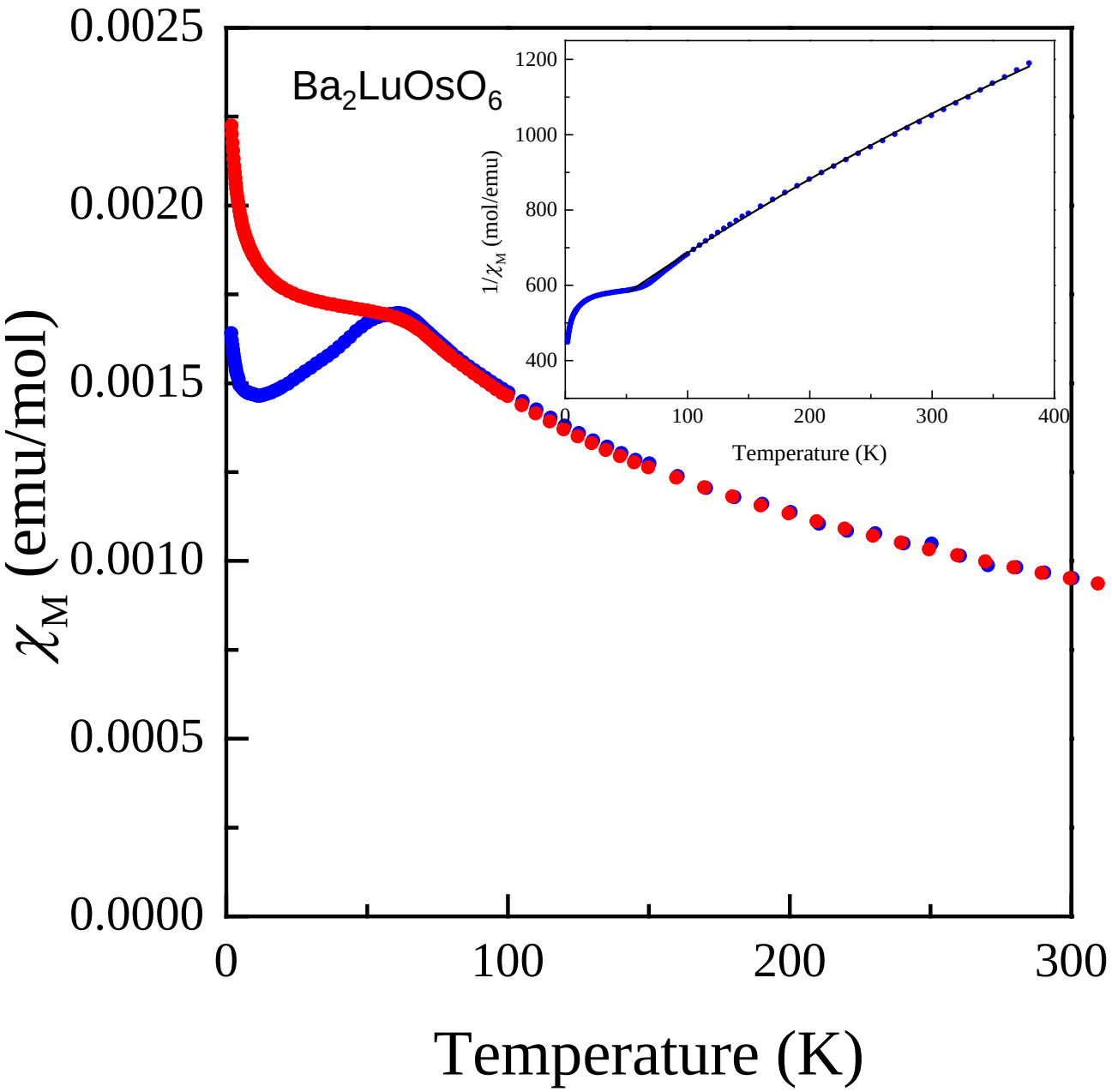
Ba2LuOsO6
0.0025
0.0020
0.0015
0.0010
0.0005
0.0000
χM (emu/mol)
0
100
200
300
Temperature (K)
1200
1000
800
600
400
1/χM (mol/emu)
0
100
200
300
400
Temperature (K)

Fig.4

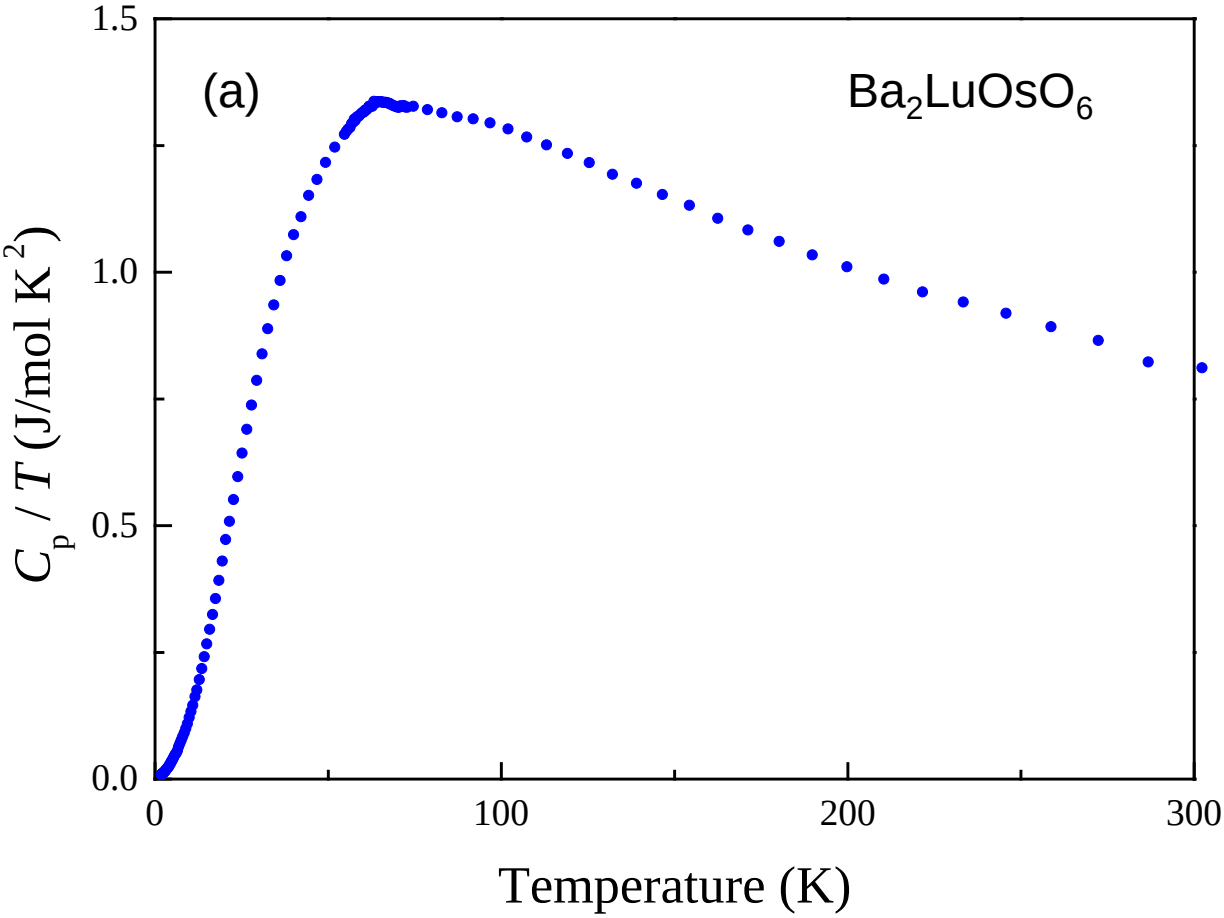
(a)
Ba_2LuOsO_6
C_p / T (J/mol K^2)
1.5
1.0
0.5
0.0
0
100
200
300
Temperature (K)

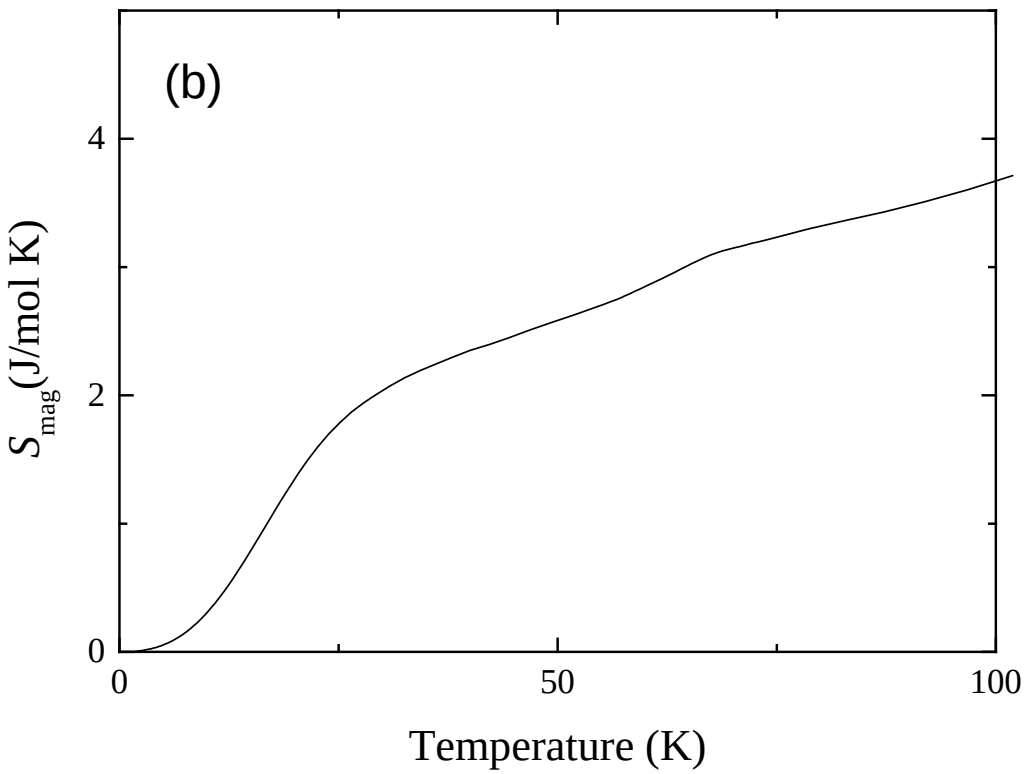
(b)
S_{mag}(J/mol K)
4
2
0
0
50
100
Temperature (K)

Fig.5

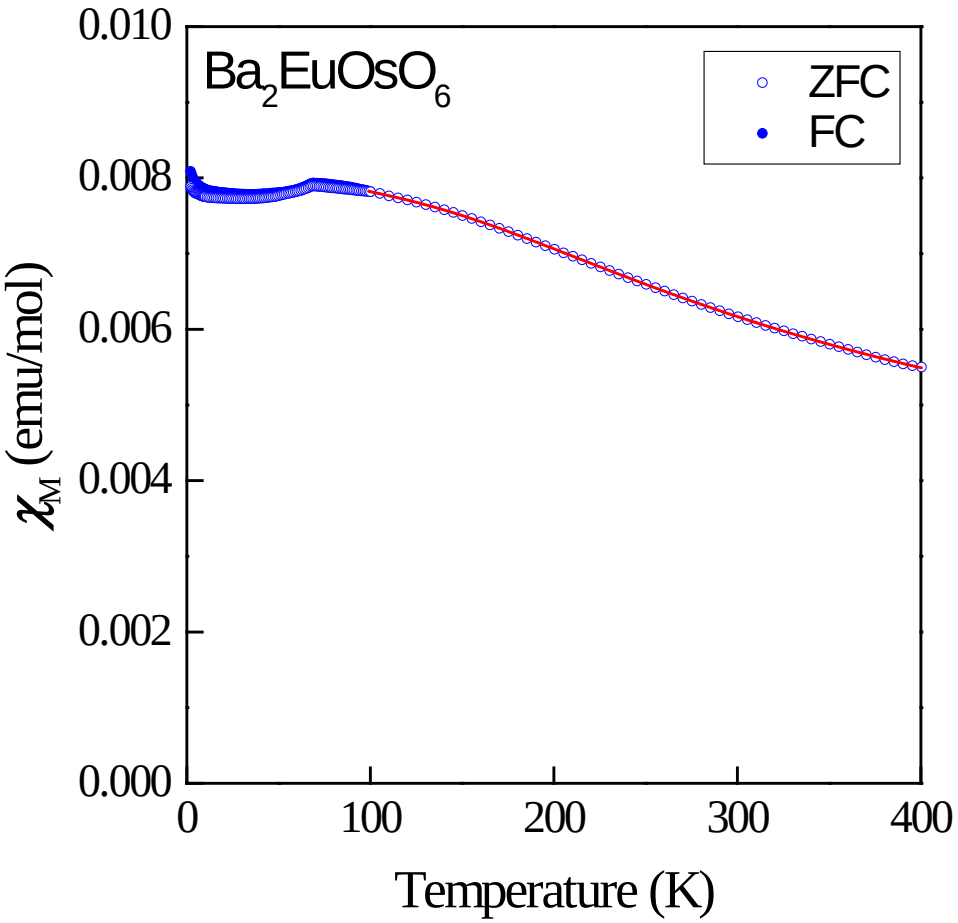
Ba2EuOsO6
ZFC
FC
0.010
0.008
0.006
0.004
0.002
0.000
χM (emu/mol)
0
100
200
300
400
Temperature (K)

Fig.6

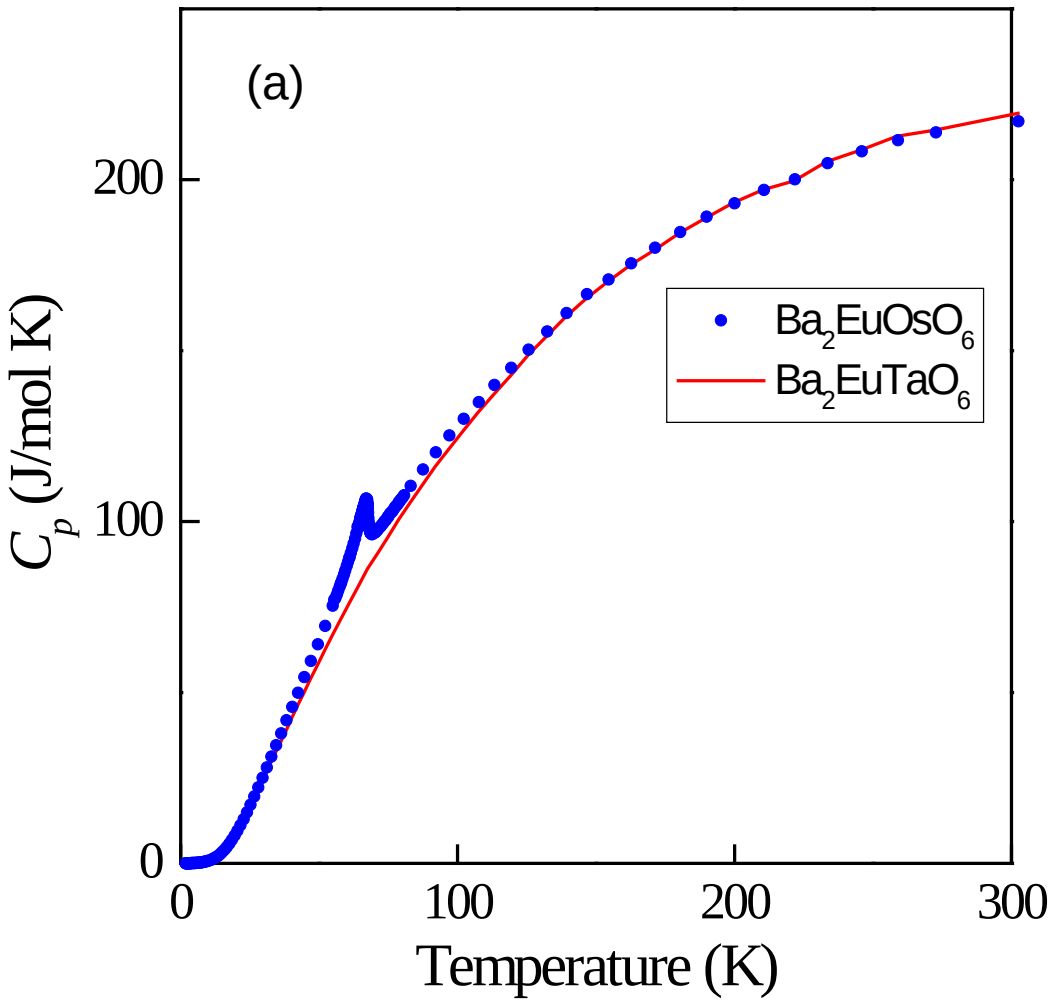
(a)
200
100
0
C_p (J/mol K)
0
100
200
300
Temperature (K)
Ba_2EuOsO_6
Ba_2EuTaO_6

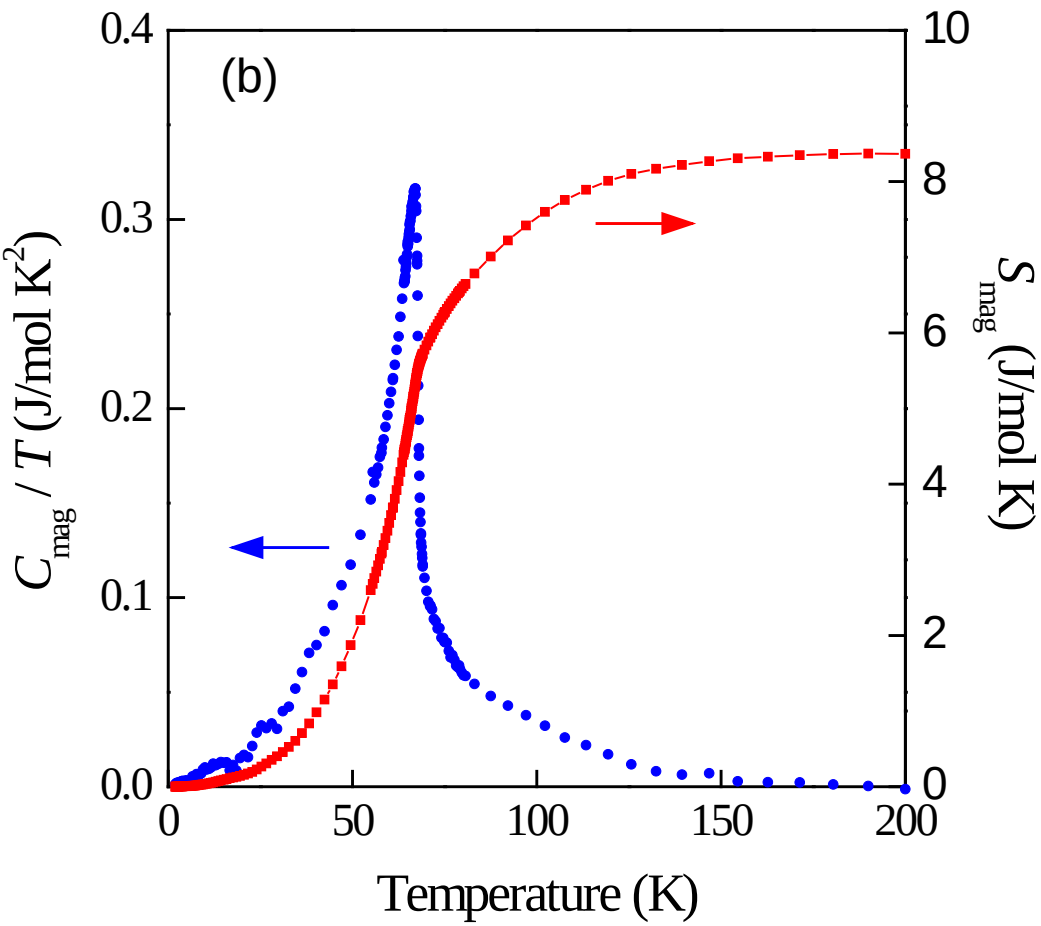
(b)
0.4
0.3
0.2
0.1
0.0
C_{mag} / T (J/mol K^2)
10
8
6
4
2
0
S_{mag} (J/mol K)
0
50
100
150
200
Temperature (K)

Fig. 7

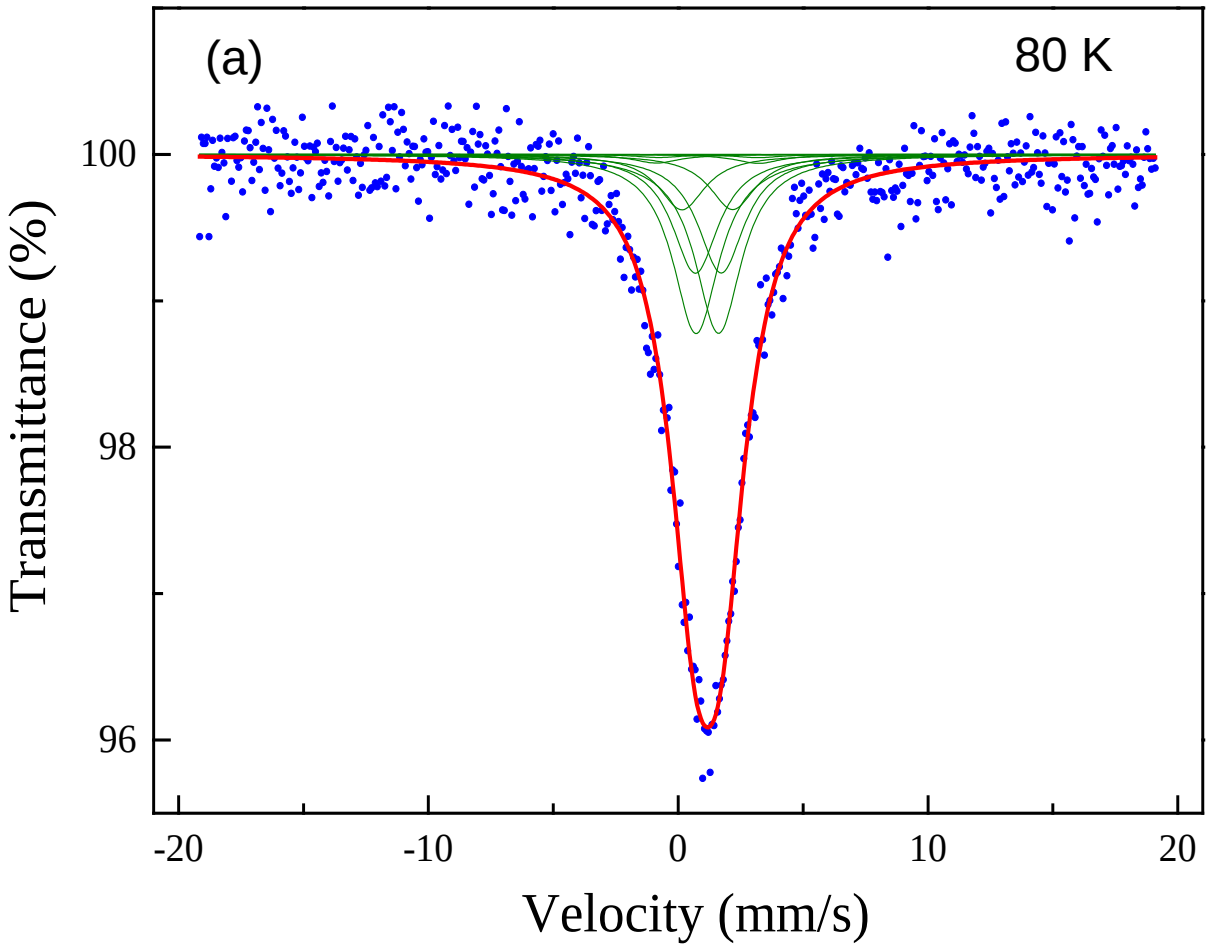
(a)
80 K
Transmittance (%)
100
98
96
-20
-10
0
10
20
Velocity (mm/s)

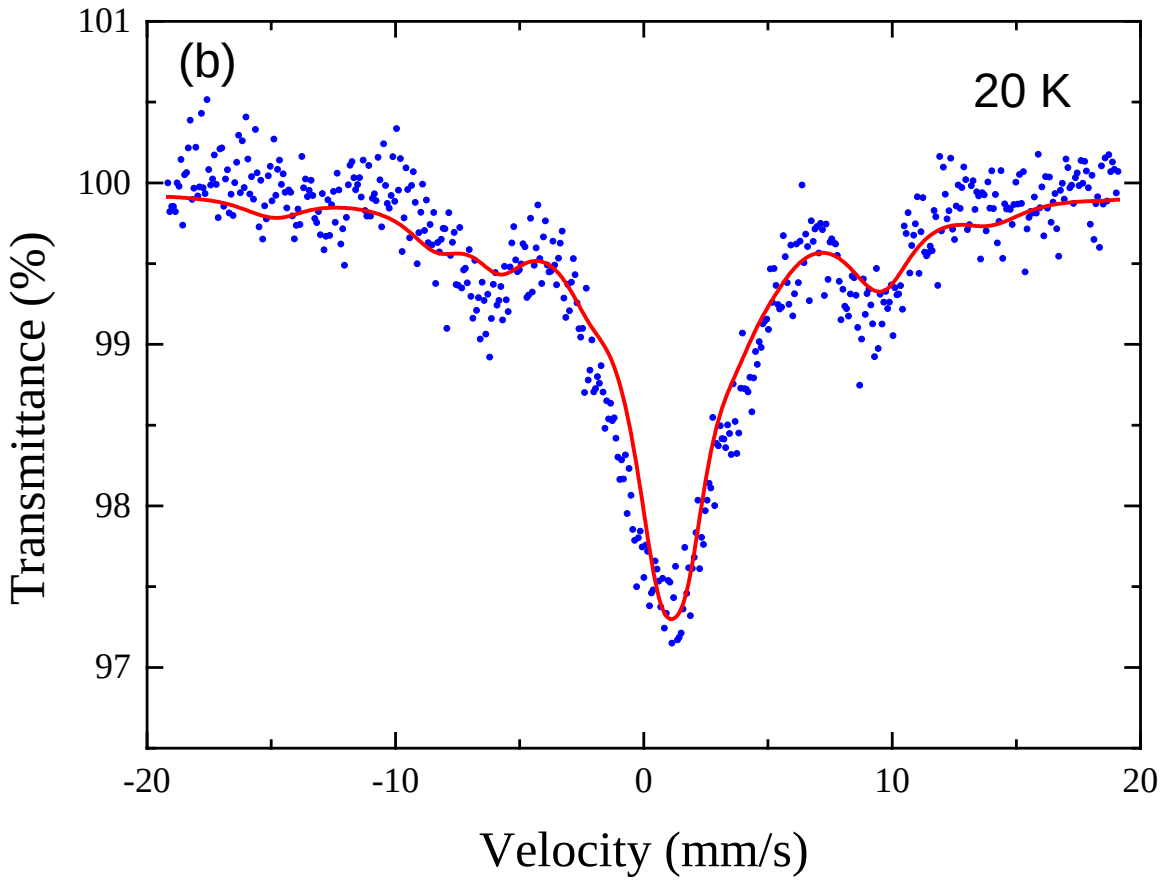
(b)
20 K
Transmittance (%)
101
100
99
98
97
-20
-10
0
10
20
Velocity (mm/s)

Fig.8

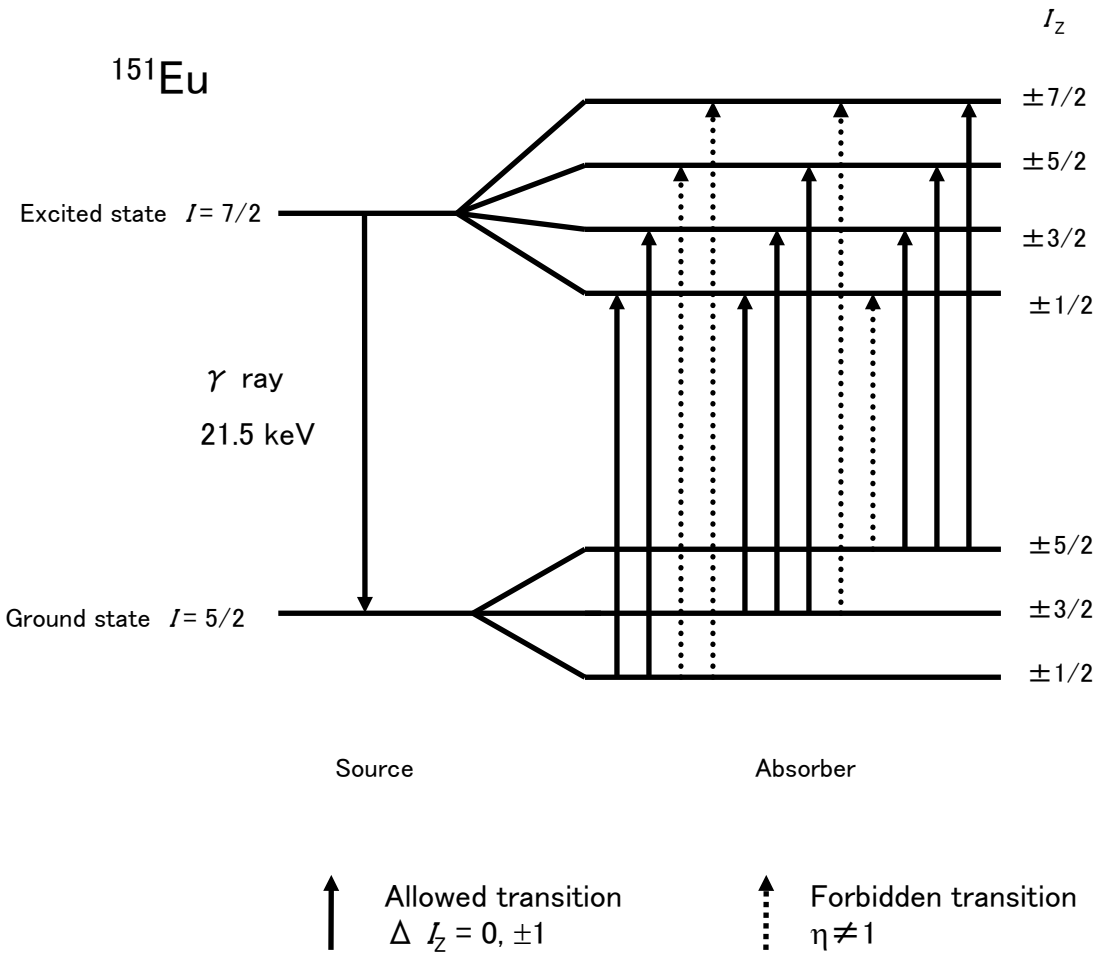
I_z
^{151}Eu
Excited state I = 7/2
γ ray
21.5 keV
Ground state I = 5/2
±7/2
±5/2
±3/2
±1/2
±5/2
±3/2
±1/2
Source
Absorber
Allowed transition
Δ I_z = 0, ±1
Forbidden transition
η≠1

Fig.9

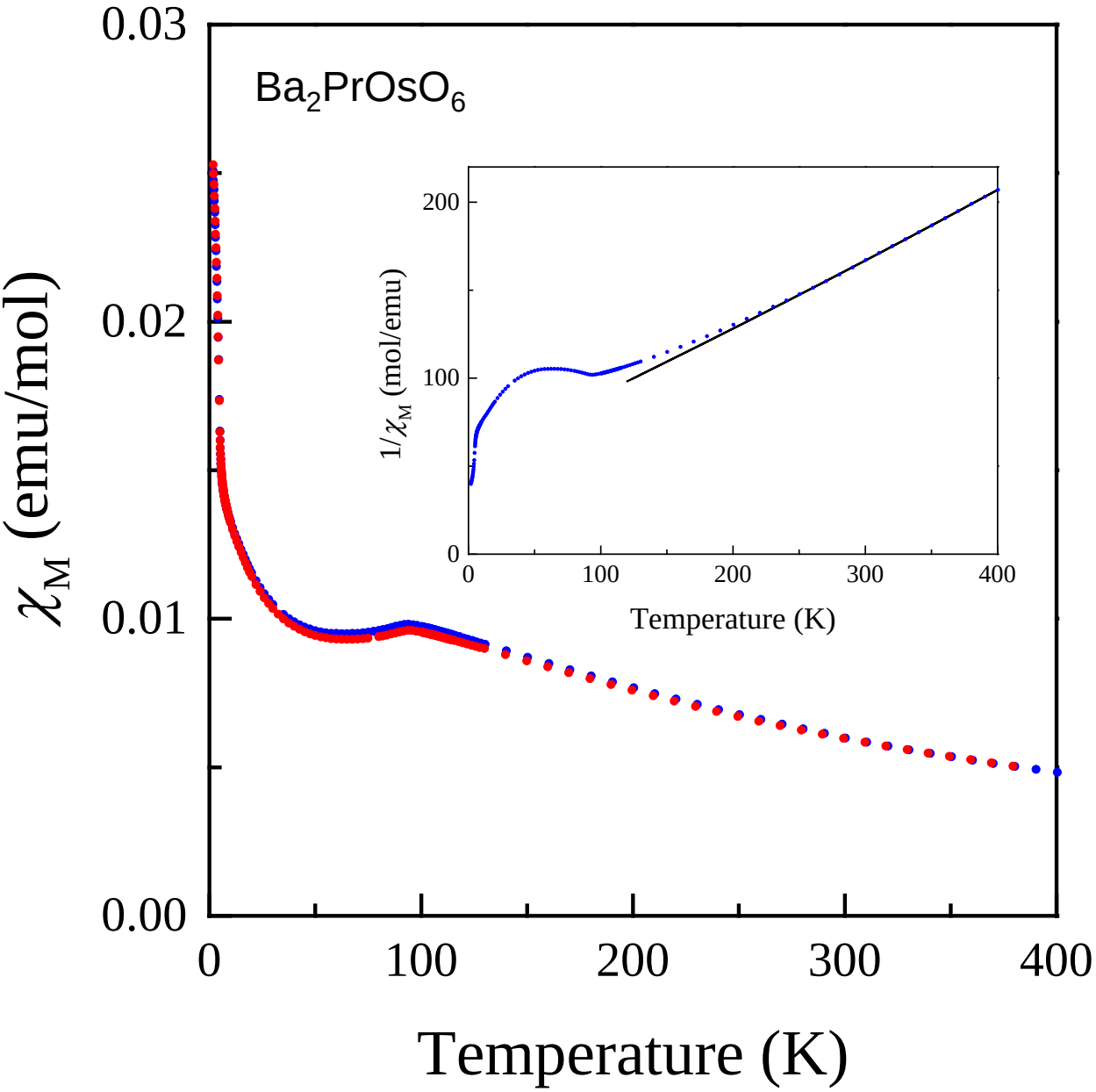
Ba2PrOsO6
χM (emu/mol)
0.03
0.02
0.01
0.00
0
100
200
300
400
Temperature (K)
1/χM (mol/emu)
200
100
0
0
100
200
300
400
Temperature (K)

Fig.10

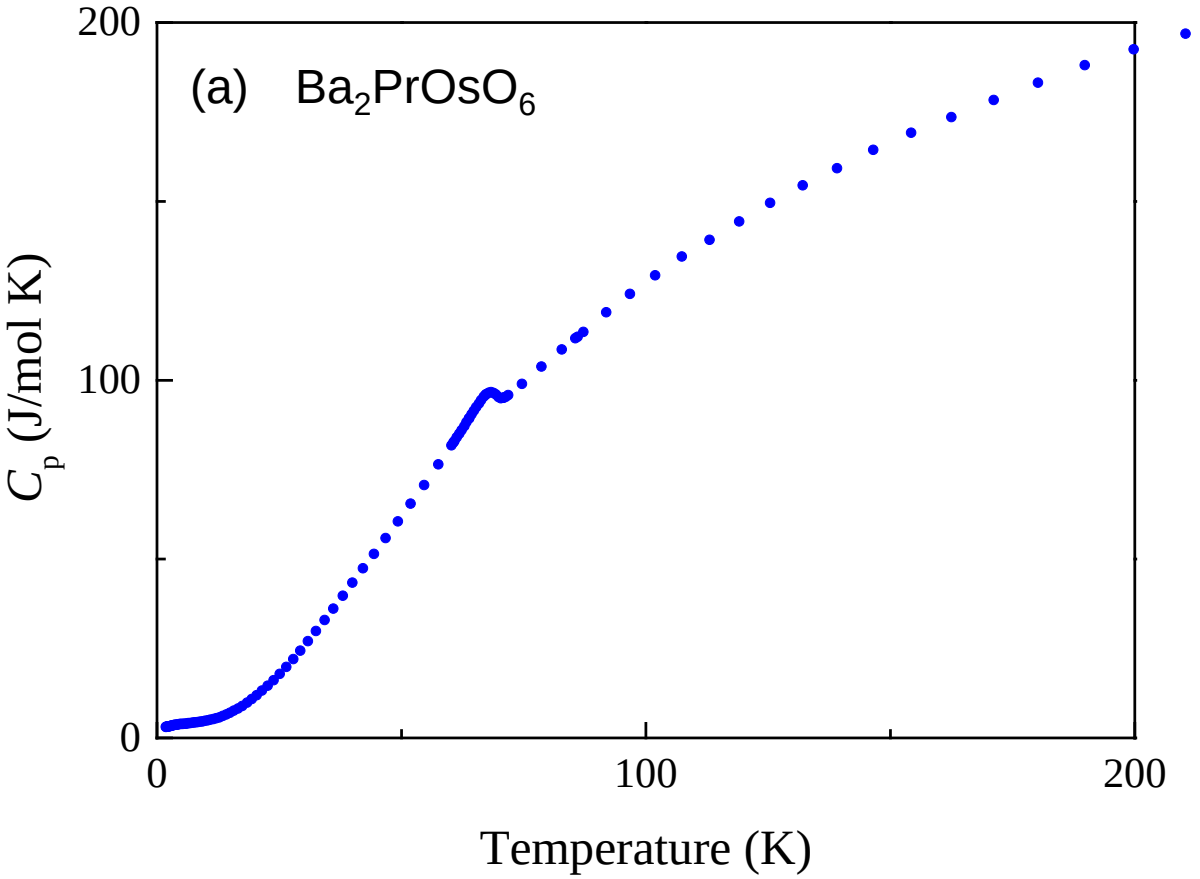
(a) Ba_2PrOsO_6
C_p (J/mol K)
200
100
0
0
100
200
Temperature (K)

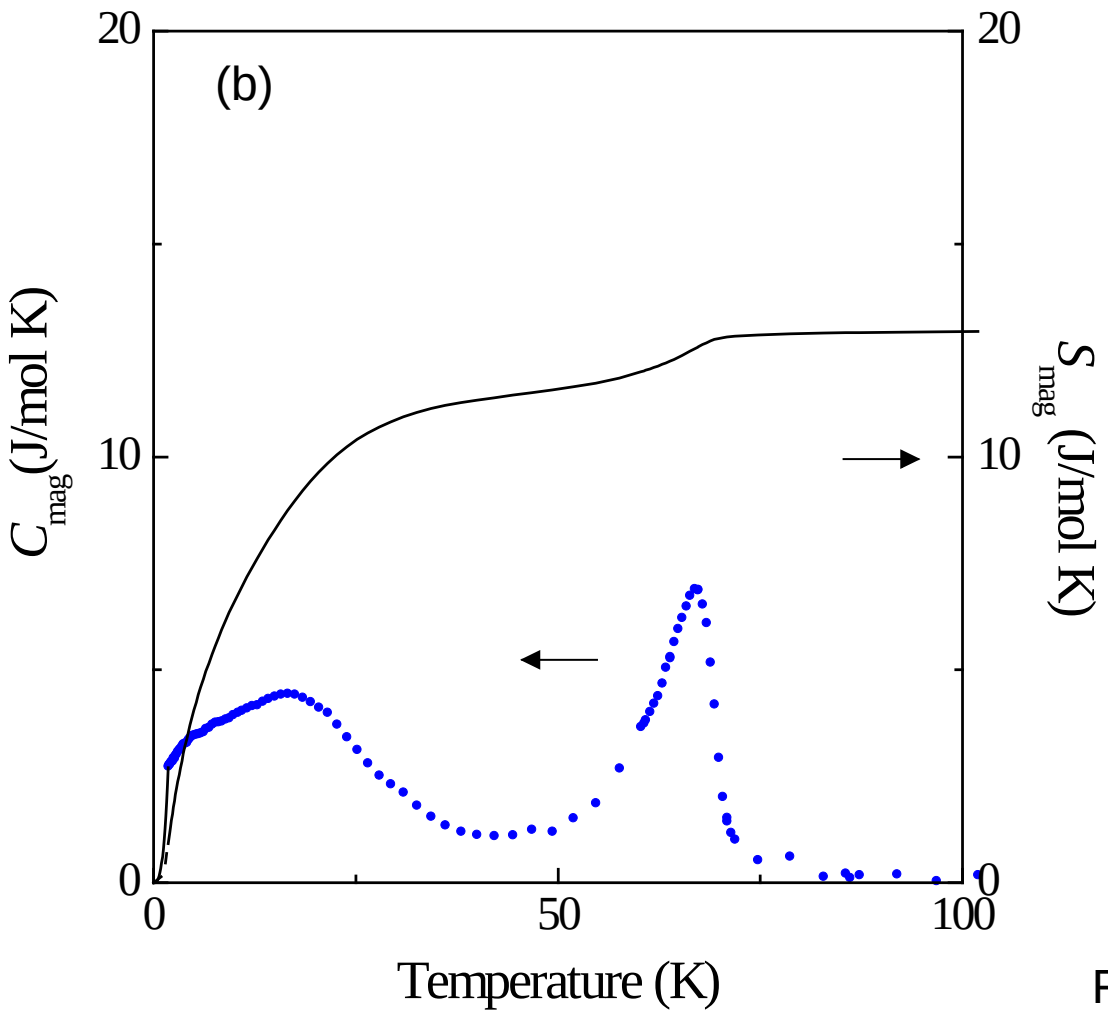
(b)
C_{mag}(J/mol K)
S_{mag} (J/mol K)
20
10
0
0
50
100
Temperature (K)

Fig.11

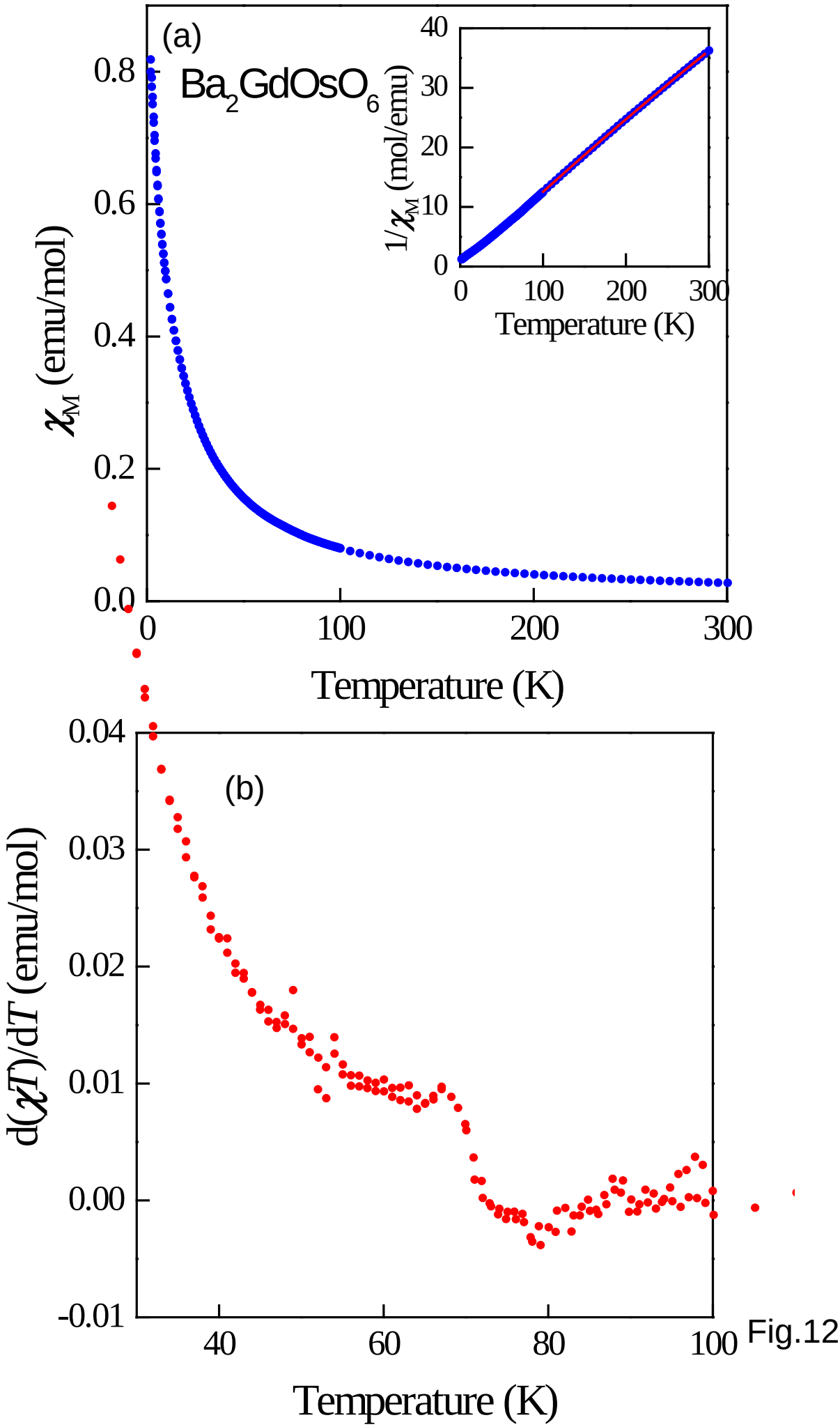
(a)
Ba_2GdOsO_6
χ_M (emu/mol)
Temperature (K)
$1/\chi_M$ (mol/emu)
Temperature (K)
(b)
$d(\chi T)/dT$ (emu/mol)
Temperature (K)

Fig.12

Table 1. Structural parameters for Ba_2SmOsO_6.

Atom	Site	*x*	*y*	*z*	B / Å^2
Ba	8*c*	1/4	1/4	1/4	0.60(2)
Sm	4*b*	1/2	1/2	1/2	0.23(3)
Os	4*a*	0	0	0	0.20(4)
O	24*e*	0.2335(11)	0	0	1.2(2)

Space group $Fm\bar{3}m$; a = 8.4505(5) Å; R_{wp} = 18.05 % and R_e = 11.02 %, where

$$R_{wp} = \left[\sum_i w_i \left(y_i - f_i(\boldsymbol{x}) \right)^2 / \sum_i w_i y_i^{\,2} \right]^{1/2} \quad \text{and} \quad R_e = \left[(N - P) / \sum_i w_i y_i^{\,2} \right]^{1/2}.$$

.

Table 2. The effective magnetic moments (μ_{eff}: experimental, μ_{calc}: calculated) per formula unit and Weiss constants for Ba_2LnOsO_6.

Ln	μ_{eff} / μ_B	μ_{calc} / μ_B [(a)]	θ / K	T_N / K
Pr	3.89	3.85	–159.5	71
Nd	3.80	3.85	–17.9	70
Sm	-		-	65
Eu	1.10 [(b)]		-71.4 [(b)]	67
Gd	8.13	8.05	–11.4	67
Tb	9.76	9.81	–21.1	2.6
Dy	10.66	10.71	–21.4	para
Ho	10.1	10.68	–7.8	24
Er	9.15	9.68	–8.9	para
Tm	7.37	7.68	–25.5	para
Yb	4.86	4.73	–106.1	2.4
Lu	1.31	1.31	–123.9	66

(a) The effective magnetic moments of Ba_2LnOsO_6 (μ_{calc}) are calculated from the equation $\mu_{calc} = \sqrt{\mu_{Os^{5+}}{}^2 + \mu_{Ln^{3+}}{}^2}$, assuming that the moment of the Os^{5+} ion is $1.31\mu_B$ (this value is obtained from Ba_2LuOsO_6, see text).

(b) These values are determined from Eq. (3) (see text).

Table 3. ^{151}Eu Mössbauer parameters for Ba_2EuOsO_6 and Ba_2EuNbO_6.

compounds	δ / (mm/sec)	$eV_{zz}Q_g$ / (mm/sec)	η
Ba_2EuOsO_6	1.12	6.21	0.78
Ba_2EuNbO_6 [(a)]	1.50	4.96	0.35

Note: δ, $eV_{zz}Q_g$, and η are isomer shift, quadrupole coupling constant, and asymmetry parameters, respectively.

(a) Reference (36).